Conformational Distributions of a Four-Way DNA Junction Revealed by Time-Resolved Fluorescence Resonance Energy Transfer†

Peggy S. Eis and David P. Millar*

The Scripps Research Institute, Department of Molecular Biology, MB20, 10666 North Torrey Pines Road, La Jolla, California 92037

Received June 21, 1993; Revised Manuscript Received September 29, 1993®

ABSTRACT: Conformational distributions of a four-way DNA junction have been examined by time-resolved fluorescence resonance energy transfer (FRET). A series of dye-labeled junctions were synthesized with donor (fluorescein) and acceptor (tetramethylrhodamine) dyes conjugated to the 5′ termini of the duplex arms in all six pairwise combinations. The fluorescence decay of the donor in each junction was measured by time-correlated single-photon counting. The distributions of donor–acceptor (D–A) distances present between each pair of arms were recovered from the donor decays using a continuous Gaussian distribution model. The overall geometry of the four-way junction defined by the six mean D–A distances was consistent with a stacked-X structure, wherein pairs of duplex arms associate to form two continuous domains. Large differences were observed in the widths of the D–A distance distributions, depending on which pair of arms were labeled with the donor and acceptor dyes. Distances measured along the stacking domains were characterized by relatively narrow distributions, indicating that these domains were rigid, whereas distances between stacking domains had broader distributions, reflecting variability in the angle between the two domains. The distances described by broad distributions were overestimated by steady-state FRET measurements. These results suggest that an ensemble of stacked-X structures are present in solution, characterized by differences in the small angle between the stacking domains. Temperature and solvent effects on the recovered distribution widths provide an indication of flexibility in the four-way junction.

Genetic recombination occurs when homologous strands are exchanged between two duplex DNA molecules. The mechanism of recombination involves formation of a four-way branched structure, the Holliday junction (Holliday, 1964), which is subsequently cleaved by cellular resolvases to yield either parental or recombinant products. The Holliday junction is an inherently mobile structure and can propagate along homologous stretches of DNA before cleavage occurs. The distribution of parental and recombinant cleavage products appears to be determined by the three-dimensional structure of the Holliday junction. Consequently, there is considerable interest in the structure of branched DNA molecules and the way in which local base sequence modulates structure [reviewed by Cooper and Hagerman (1991) and Lilley and Clegg (1993)]. Most physical studies have concentrated on Holliday junction analogs formed from four synthetic oligonucleotides in which the base sequence is designed to immobilize the position of the branch point (Seeman, 1982; Seeman & Kallenbach, 1983). These stable four-way DNA junctions have been studied by a variety of techniques including gel electrophoresis (Cooper & Hagerman, 1987; Duckett et al., 1988), chemical footprinting (Churchill et al., 1988; Guo et al., 1990), transient electric birefringence (Cooper & Hagerman, 1989), NMR spectroscopy (Wemmer et al., 1985; Chen et al., 1991, 1993), fluorescence resonance energy transfer (Murchie et al., 1989; Cooper & Hagerman, 1990), and molecular modeling (von Kitzing et al., 1990). It is now well established that the four-way junction folds into an "X" shape in the presence of cations, with two continuous domains formed by pairwise stacking between junction arms.

The experimental approaches used in biophysical studies of the four-way junction have not provided direct structural data on this complex. Consequently, it is unknown whether the four-way junction actually adopts a unique structure in solution, or whether an ensemble of different structures are possible. Fluorescence resonance energy transfer (FRET)[1] from a donor to an acceptor chromophore has been used to estimate distances in nucleic acid structures (Beardsley & Cantor, 1970; Yang & Söll, 1974; Cardullo et al., 1988). Steady-state measurements of energy transfer, based on the integrated emission intensity of the donor or acceptor, have been used to determine relative distances between the arms of a dye-labeled four-way DNA junction (Murchie et al., 1989; Cooper & Hagerman, 1990). However, steady-state measurements of FRET do not establish that the duplex arms adopt a unique spatial arrangement. Time-resolved measurements of FRET are informative in this regard, since the time course of the donor's fluorescence decay is very sensitive to dispersion in the donor–acceptor (D–A) distance. We have previously used time-resolved energy transfer to recover the distribution of end-to-end distances in a dye-labeled DNA duplex (Hochstrasser et al., 1992). Time-resolved energy transfer has also been used to recover intramolecular distance distributions in peptides (Eis & Lakowicz, 1993), proteins

† Supported by a grant from the National Science Foundation (MCB-9019250 to D.P.M.).

* Corresponding author.

® Abstract published in *Advance ACS Abstracts,* November 15, 1993.

[1] Abbreviations: A, energy-transfer acceptor; D, energy-transfer donor; F, fluorescein; FRET, fluorescence resonance energy transfer; fwhm, full width of the distribution at half-maximum probability; R, tetramethylrhodamine; R_0, critical transfer distance for donor–acceptor energy transfer; $\bar{R}$, mean donor–acceptor distance.

0006-2960/93/0432-13852$04.00/0

(Amir & Haas, 1987; Lakowicz et al., 1988), and carbohydrates (Wu et al., 1991).

In the present study, we have used time-resolved energy transfer to examine the conformational distribution of a four-way DNA junction. We have synthesized a series of four-way junctions with fluorescent donor and acceptor dyes attached to the 5′ termini of the duplex arms in all six pairwise combinations. By analyzing the fluorescence decay of the donor in each junction, we have been able to estimate the range of distances present between each pair of arms in the four-way junction. With these data we are able to judge whether the four duplex arms adopt a unique spatial arrangement or, alternatively, to characterize the ensemble of junction structures present in solution. Finally, by examining the effects of temperature and solvent viscosity on the donor decays, we can probe the flexibility of the four-way junction.

MATERIALS AND METHODS

Oligonucleotide Synthesis and Dye Labeling. Oligonucleotides were synthesized on an Applied Biosystems DNA synthesizer (Model 108B) using β-cyanoethyl phosphoramidite chemistry. A 5′-aminohexyl phosphate linker was attached to each oligonucleotide during a final synthesis cycle using 6-[(trifluoroacetyl)amino]hexyl methyl *N*,*N*-diisopropylphosphoramidite. Oligonucleotides were cleaved and deprotected using standard methods.

Donor- and acceptor-labeled DNA strands were prepared by reacting the crude 5′-amino oligonucleotides with succinimidyl ester derivatives (Molecular Probes) of 5-carboxyfluorescein (donor) or 5-carboxytetramethylrhodamine (acceptor). A 30–50-fold molar excess of dye (0.2 mg of dye/μL of dimethylformamide) was added to a 2 mM solution of crude oligonucleotide in 0.1 M $NaHCO_3$, pH 9. Reactions were performed in the dark at room temperature overnight. Unreacted dye was removed on a 10-mL Sephadex G-25 column. Dye-labeled and unlabeled 5′-amino oligonucleotides were purified by reverse-phase HPLC using a Vydac C_{18} column (1 × 25 cm) and gradient elution with a 0.1 M triethylammonium acetate/acetonitrile eluent system. Strand purity was confirmed by analytical HPLC using a C_{18} column (0.46 × 25 cm) and the same eluent system.

The base sequences of the four oligonucleotides comprising the four-way junction are shown in Chart I. The junction was derived from the J1 junction of Kallenbach et al. (1983) with replacement of the 5′-terminal C nucleotide with T, and the 3′-terminal G nucleotide with A, in each strand. These changes were necessary in order to minimize local dye–DNA quenching interactions (Millar et al., 1992).

Junction Formation. Donor-only, acceptor-only, and D–A four-way DNA junctions were prepared by mixing the appropriate strands in a buffer containing 20 mM Tris, 50 mM NaCl, 5 mM $MgCl_2$, and 0.2 mM EDTA at pH 7.5. Concentrations of unlabeled and labeled oligonucleotides were estimated by the 260-, 496- (fluorescein), or 558-nm absorbance (tetramethylrhodamine). In donor-only junctions, the concentration of the donor strand was 0.5 μM and the concentration of each unlabeled strand was 1.5 μM. The excess of unlabeled strands ensured that all donor strands were annealed into four-way junctions. In acceptor-only junctions, the acceptor strand concentration was 0.5 μM and the concentration of each unlabeled strand was 1.5 μM. In the D–A junctions, the concentration of donor strands was 0.5 μM and the concentration of the acceptor strand and each of the two unlabeled strands was 1.5 μM. Dye-labeled junctions are referred to by specifying the dye(s) and the labeled strand(s): for example, F1 refers to a singly labeled junction in which fluorescein is attached to strand 1, while F1R2 refers to a doubly labeled junction in which fluorescein is attached to strand 1 and tetramethylrhodamine is attached to strand 2. The DNA strands were annealed into four-way junctions by heating the solutions at 70 °C for 5 min and then slowly cooling to room temperature.

Chart I. Base Sequence of the Four-Way DNA Junction Examined in the Present Study[a]

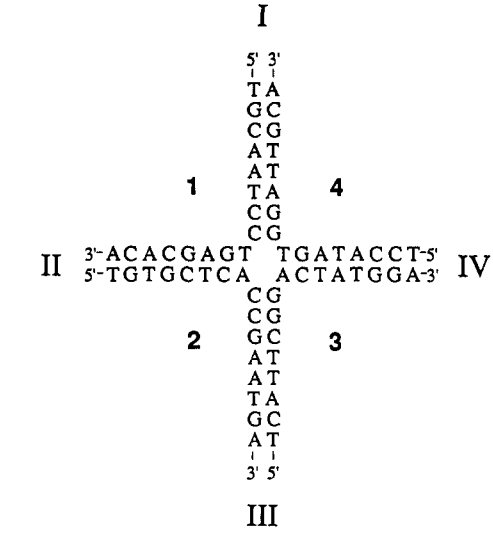

[a]The oligonucleotide strands are labeled 1–4, and the junction arms are labeled I–IV. The 5′ ends of each strand contain an aminohexyl moiety for covalent attachment of donor and acceptor dyes.

Polyacrylamide Gel Electrophoresis. Electrophoresis of donor-only and D–A junctions was performed using a 20% polyacrylamide gel containing 11 mM $MgCl_2$ and 5% glycerol. The sample buffer has been mentioned above. The running buffer was tris–borate/EDTA, pH 8.0 (Bio-Rad). Dye-labeled species were visualized under a UV lamp. Single strands, four-way junctions, and alternative oligomeric species were identified on the basis of their different electrophoretic mobilities.

Quantum Yield Determination. The quantum yields of donor-only junctions were determined using fluorescein in 0.1 N NaOH as a standard [$\phi = 0.90$ (Demas & Crosby, 1971)]. Steady-state emission spectra of the junction and reference were measured on an SLM SPF500C spectrofluorimeter with excitation at 490 nm. The quantum yield of the donor was calculated from its absorbance and integrated emission intensities relative to those of the reference.

Critical Transfer Distance. The critical transfer distance, R_0, was determined from the spectral properties of the donor and acceptor chromophores according to eq 1 (Förster, 1949),

$$R_0^6 = \left\{\frac{9000(\ln 10)\kappa^2\phi_D}{128\pi^5 N n^4}\right\}\int_0^\infty F_D(\lambda)\epsilon_A(\lambda)\lambda^4\,d\lambda \qquad (1)$$

where κ^2 is the factor that describes the orientational dependence of energy transfer, ϕ_D is the fluorescence quantum yield of the donor, N is Avogadro's number, n is the refractive index of the medium separating the donor and acceptor, $F_D(\lambda)$ is the donor fluorescence intensity at wavelength λ, and $\epsilon_A(\lambda)$ is the extinction coefficient of the acceptor at the same wavelength.

Steady-State Energy Transfer. Steady-state donor fluorescence emission was measured on an SLM SPF500C spectrofluorimeter with excitation at 490 nm. The emission intensity at the wavelength of maximum donor emission (528 nm) was measured in donor-only ($\bar{I}_D$) and D–A junctions ($\bar{I}_{DA}$).

The energy-transfer efficiency (E) was calculated from eq 2 after correction for the differential donor absorption of the two samples,

$$E = 1 - (\bar{I}_{DA}/\bar{I}_{D}) \quad (2)$$

The apparent D–A distance, R_{ss}, was calculated from eq 3,

$$R_{ss} = R_0(E^{-1} - 1)^{1/6} \quad (3)$$

Time-Resolved Fluorescence Spectroscopy. Donor or acceptor dyes were repetitively excited at 514.5 nm with 90-ps-duration pulses from a mode-locked argon ion laser (Coherent Innova 100-12). An external pulse selector reduced the pulse-repetition frequency from 78 to 1.87 MHz. Fluorescence was collected at 90° to the excitation beam, passed through a polarizer, and focused onto the entrance slit of a 0.1-m single-grating monochromator (JY H-10). The emission polarizer was oriented at 54.7° relative to the vertical excitation polarization for measurement of isotropic fluorescence decay curves, or alternated between vertical and horizontal orientations for measurement of fluorescence anisotropy decays. Donor emission was monitored at 530 nm, and acceptor emission was monitored at 580 nm. Fluorescence was detected using a microchannel plate photomultiplier (Hamamatsu R2809U-01), and its output was processed with a time-correlated single-photon counting system. Decay curves were collected in a multichannel analyzer (Ortec-Norland, Model 5510) until at least 10 000 single-photon counts had been accumulated in the peak channel. The instrument response function (fwhm = 100 ps) was measured using a dilute solution of nondairy coffee creamer to scatter the laser pulses. Most experiments were performed at 20 °C, except for the F1R4 junction, where fluorescence decays were measured at several temperatures between 5 and 30 °C.

Fluorescence Lifetimes of Donor-Only and Acceptor-Only Junctions. The fluorescence decays of donor-only or acceptor-only junctions were analyzed according to eqs 4 and 5,

$$I(t) = g(t) \otimes K(t) \quad (4)$$

and

$$K(t) = \sum_{i=1}^{N} \alpha_i \exp(-t/\tau_i), \quad (5)$$

where $I(t)$ is the isotropic fluorescence intensity at time t after excitation, $g(t)$ is the instrument response function, $\otimes$ denotes convolution of two functions, α_i is the fractional amplitude associated with each donor or acceptor lifetime τ_i, and N is the number of lifetimes. The method of nonlinear least-squares (Bevington, 1969) was used to adjust the parameters α_i and τ_i to obtain a best fit. The goodness of fit was judged by the reduced χ-square value, χ_R^2, and by examination of the weighted residuals. The average fluorescence lifetime of the donor or acceptor dyes was calculated from eq 6,

$$\bar{\tau} = \sum_{i=1}^{N} \alpha_i \tau_i \quad (6)$$

Rotational Mobility of Donor and Acceptor Dyes. The rotational mobility of the dyes was determined by time-resolved fluorescence anisotropy measurements. Fluorescence decay curves measured with the emission polarizer oriented either parallel, $I_{\parallel}(t)$, or perpendicular, $I_{\perp}(t)$, to the excitation polarization were analyzed according to eqs 7 and 8,

$$I_{\parallel}(t) = g(t) \otimes [\{1 + 2r(t)\}K(t)] \quad (7)$$

and

$$I_{\perp}(t) = g(t) \otimes [\{1 - r(t)\}K(t)] \quad (8)$$

where the time-dependent fluorescence anisotropy, $r(t)$, is represented by

$$r(t) = \sum_{k=1}^{2} r_{0k} \exp(-t/\phi_k) \quad (9)$$

and $K(t)$ is defined in eq 5. In eq 9, r_{01} and ϕ_1 are the limiting anisotropy and decay time associated with local rotation of the dyes, while r_{02} and ϕ_2 are the corresponding quantities describing overall rotation of the dye-labeled junctions. These parameters were optimized for a simultaneous best fit to $I_{\parallel}(t)$ and $I_{\perp}(t)$ (Cross & Fleming, 1984), with the parameters in the expression for $K(t)$ kept fixed at the values determined from the isotropic fluorescence decay. The goodness of fit was judged as described above. The total limiting anisotropy, r_0, is given by $r_0 = r_{01} + r_{02}$.

Orientation Factor for Energy Transfer. Since the orientations of the donor and acceptor transition dipoles within the dyes are unknown, the precise value of κ^2 is only known in the limit of free dye rotation ($\kappa^2 = 2/3$). However, the rotation of the dyes linked to DNA is hindered (Hochstrasser et al., 1992), and consequently κ^2 can have a range of values. The minimum (κ_1^2) and maximum (κ_2^2) values defining the range of most probable values for the orientation factor were obtained from Table III of Haas et al. (1978) based on the values of r_{02} determined from fluorescence anisotropy decay of the donor and acceptor dyes.

Donor–Acceptor Distance Distributions. The fluorescence decay of the donor in D–A junctions, $I_{DA}(t)$, was analyzed according to eq 10,

$$I_{DA}(t) = g(t) \otimes [(1-f)\int_{R_{min}}^{R_{max}} \sum_i \alpha_i \exp\{(-t/\tau_i)[1 + (R_0/R)^6]\}P(R)\,dR] + fI_D(t) \quad (10)$$

wherein the probability distribution of D–A distances, $P(R)$, is assumed to be static on the time scale at which energy transfer occurs; R_{min} is the distance of closest approach of the donor and acceptor; and R_{max} is the maximum D–A distance. The intrinsic donor lifetimes, τ_i, and amplitudes, α_i, were obtained from the decay of donor-only junctions, as described above, and were kept constant in the analysis of the D–A junctions. The first term in eq 10 describes the decay of donors that undergo energy transfer to the acceptor, while the second term accounts for a fraction (f) of donors that do not undergo energy transfer because of incomplete junction formation. $I_D(t)$ describes the decay of the donor in the absence of the acceptor. The D–A distance distribution was described by a continuous Gaussian distribution of distances in three dimensions (Haas et al., 1975):

$$P(R) = 4\pi R^2 c \exp(-a(R-b)^2) \quad \text{for } R_{min} < R < R_{max}$$
$$= 0 \quad \text{elsewhere} \quad (11)$$

where a and b are adjustable parameters and c is a normalization constant. Equation 10 was used to fit the donor decays in the D–A junctions by optimizing the parameters a and b in eq 11 and the fraction of free donor species (f). The goodness of fit was judged as described above. The resulting D–A distance distributions were calculated form eq 11 using the best-fit values of a and b. The mean D–A distance ($\bar{R}$) was evaluated as the first moment of the recovered distribution. The full width of the distribution at half-maximum probability (fwhm) was also evaluated.

Table I: Effect of Sample Composition on the Fraction of Free Donor Species and Recovered Distance Distribution Parameters for Junction F1R3

[A]/[D][a]	% free donor[b]	$\bar{R}$ (Å)[c]	fwhm (Å)[c]
0.63	42.9	57.1	16.4
0.72	35.1	57.4	18.0
0.84	23.8	57.3	19.5
0.91	17.4	57.0	18.9
1.00	13.1	57.3	19.1
1.20	8.3	56.8	18.0
1.33	3.3	57.4	20.3
2.00	1.3	56.9	20.0
average		57.2	18.7

[a] Molar ratio of acceptor and donor strands in the sample; concentrations of the two unlabeled strands were equal to that of the acceptor strand in all junction samples. [b] Percentage of free donors in the sample, 100f, where f was obtained by fitting eq 10 to the donor decay. [c] Parameters describing the D–A distance distributions recovered for each sample; $\bar{R}$ is the mean D–A distance, and fwhm is the full width of the distribution at half-maximum probability.

Equation 10 assumes a single value for the orientation factor (R_0 is calculated from eq 1 with $\kappa^2 = 2/3$). Orientational effects on energy transfer were included by also averaging the donor decay over the range of possible values for the orientation factor (Albaugh & Steiner, 1989),

$$I_{DA}(t) = g(t) \otimes \left[\frac{(1-f)}{(\beta_2 - \beta_1)} \int_{\beta_1}^{\beta_2} \int_{R_{min}}^{R_{max}} \sum_i \alpha_i \exp\{-(t/\tau_i)[1 + (\beta R_0/R)^6]\} P(R)\, dR\, d\beta \right] + f I_D(t) \quad (12)$$

where $\beta = (3/2)\kappa^2$. Note that R_0 in eq 12 is calculated from eq 1 with $\kappa^2 = 2/3$ and that β scales the value of R_0^6 accordingly; β_1 and β_2 correspond to κ_1^2 and κ_2^2, respectively.

RESULTS

Homogeneity of Dye-Labeled Oligonucleotides. Analytical HPLC of the purified dye-labeled oligonucleotides revealed a single sharp peak absorbing at both 260 and 496 nm (fluorescein) or 558 nm (tetramethylrhodamine). Measurement of the absorbances at these wavelengths confirmed that these species contained one dye per oligonucleotide strand.

Formation of Four-Way Junctions. Since D–A distance distributions were recovered solely from the fluorescence decay of the donor, it was important to ensure that all the donor strands were annealed in four-way junctions. To establish the appropriate experimental conditions, we determined the amount of free donor species present in solutions containing various mixtures of the four complementary oligonucleotides. Annealed and free donor species were distinguished on the basis of their different fluorescence decay behaviors, since annealed donor strands decayed more rapidly than free donor strands because of energy transfer to the acceptor. We found that by analyzing donor decays according to eq 10, which contains separate terms for annealed and free donor species, we could detect free donor species comprising as little as 1% of the total donor population in a junction sample (Table I). We first verified that the parameter f in eq 10 reported the fraction of free donor species by examining a series of F1R3 samples that contained known amounts of free donor strands; these were prepared with <1 molar equiv of the three complementary oligonucleotides relative to the F1 donor strand. The f values recovered for these samples correlated with the expected fraction of free donor strands (Table I). Thus, it was apparent that an equimolar mixture of the four complementary oligonucleotides contained a significant amount (13%) of free donor species (Table I). As shown in Table I, >1 molar equiv of the acceptor-labeled and the two unlabeled oligonucleotides was needed to reduce the amount of free donors to an acceptable level. This probably reflects errors in the estimated concentrations of the strands, although it may also reflect in part the thermodynamic stability of the four-way junction in our samples. We note that the replacement of four G·C base pairs with A·T pairs, required to reduce local dye quenching at the arm termini, will reduce the stability of the four-way junction relative to the parental J1 sequence. Nevertheless, it is clear that complete annealing of the donor strand into four-way junctions could be achieved by adding an excess of the other three strands.

Table II: Lifetime Analysis of Donor-Only Junctions[a]

junction[b]	τ_1 (ns) (±0.05)	τ_2 (ns) (±0.03)	α_1 (±0.005)	α_2 (±0.005)	$\bar{\tau}$ (ns)[c] (±0.02)
F1 or F2	1.26	5.04	0.069	0.931	4.78
F3	1.70	4.62	0.047	0.953	4.48

[a] Isotropic decays of donor fluorescence were analyzed according to eqs 4 and 5 with two lifetime components. [b] Junctions contained the indicated fluorescein-labeled (F) strand plus a 3-fold molar excess of unlabeled strands. F1 and F2 lifetimes are equivalent. [c] Average fluorescence lifetime calculated from eq 6.

On the basis of these observations, all junction samples were prepared with a 3-fold molar excess of acceptor-labeled and unlabeled strands relative to the donor-labeled strand. The presence of excess acceptor-labeled and unlabeled strands did not complicate the interpretation of the results, since only the donor-labeled strand was observed in the fluorescence decay measurements. This was confirmed by the D–A distance distributions recovered for each junction sample in Table I. The parameters describing these distributions, the mean D–A distance ($\bar{R}$) and the width of the distribution (fwhm), were independent of the relative amounts of the junction strands. Therefore, energy transfer was occurring within the same complex, regardless of the composition of the junction samples. We confirmed that this complex was actually a four-way junction by examining the F1R3 samples by polyacrylamide gel electrophoresis.

As a final check of junction formation, the fraction of free donor species (f) was freely optimized when eq 10 or 12 was fit to the donor decays in each D–A junction sample. The recovered values of this parameter were in the range 0–0.02 for all junction samples, confirming that the donor strand was always completely annealed into four-way junctions, regardless of which strands were labeled with the donor and acceptor dyes.

Fluorescence Lifetimes of Donor-Only Junctions. Lifetime analyses of donor-only junctions are listed in Table II. The best fit to the fluorescence decay in each donor-only junction was obtained with two fluorescence lifetimes: the major lifetime was similar to the lifetime of free fluorescein under the same conditions, whereas the minor lifetime was shorter than the free dye lifetime. These results indicate that a small population of donors (~5%) were quenched because of dye–DNA interactions (Millar et al., 1992). The average fluorescence lifetimes of junctions F1 and F2 were identical. Likewise, the quantum yields of donor emission in these two junctions were equivalent (0.45). The average donor lifetime in junction F3 was slightly shorter than in F1 or F2, and the quantum yield was also lower (0.39). This difference in quantum yields affects the critical transfer distance (R_0) in the corresponding D–A junctions: R_0 = 54.3 Å for D–A junctions with donor labeling at strands 1 or 2 and R_0 = 53.2 Å for D–A junctions with the donor attached to strand 3. We

Table III: Anisotropy Decay Parameters for Donor-Only and Acceptor-Only Junctions[a]

junction[b]	ϕ_1 (ns) (±0.05)	ϕ_2 (ns) (±0.2)	r_{01} (±0.005)	r_{02} (±0.005)	r_0 (±0.01)	θ (deg)[c] (±1.0)
F1	0.51	11.8	0.168	0.180	0.35	36.9
F2	0.59	11.9	0.164	0.176	0.34	36.9
F3	0.51	11.6	0.158	0.192	0.35	35.4
R2	0.55	14.2	0.153	0.236	0.39	32.4
R3	0.59	14.4	0.145	0.238	0.38	31.6
R4	0.54	14.7	0.136	0.253	0.39	30.2

[a] Fluorescence anisotropy decay data were analyzed according to eqs 7–9. [b] Each sample contained the donor (F) or acceptor (R) strand indicated plus a 3-fold molar excess of each unlabeled strand. [c] Chromophore's cone semi-angle, calculated from eq 11 of Hochstrasser et al. (1992).

note that it was not necessary to use a different R_0 value for each individual lifetime component in calculating D–A distance distributions from eqs 10 or 12; the recovered distributions were the same regardless of whether a single R_0 value was used for both components or whether the R_0 values were scaled according to the individual lifetimes (Albaugh & Steiner, 1989).

In a previous fluorescence decay study, the dye–DNA interactions were shown to be sensitive to the identity of the 5′-terminal base at the site of dye attachment (Millar et al., 1992). In each of the donor junctions in Table II, the labeled strand contained thymine at the 5′ terminus. However, junction F3 contained cytosine as the penultimate 5′ base, whereas F1 and F2 both contained guanine at this position. The small differences in the donor lifetimes of F1 and F2 compared with F3 suggest that dye quenching is also influenced to some extent by the penultimate 5′-terminal base. Use of the appropriate donor-only junction as reference for a given D–A energy-transfer measurement should obviate any bias in the recovered distance distribution resulting from these small differences.

Rotational Mobility of Donor and Acceptor Dyes. Time-resolved fluorescence anisotropy decay measurements were performed on donor-only and acceptor-only junctions to determine the rotational mobility of each dye. These results are summarized in Table III. The fluorescence anisotropy decays in all donor-only and acceptor-only junctions were well represented by two rotational correlation times according to eq 9 (χ_R^2 = 1.0–1.2). The shorter correlation time, reflecting local rotation of the dyes, had approximately the same value (500–600 ps) in each donor-only and acceptor-only junction. The longer correlation time associated with global rotation of the junction was ~12 ns for all donor-labeled junctions and ~14 ns for all acceptor-labeled junctions. The small difference in ϕ_2 for the donor-only and acceptor-only junctions probably reflects a different orientation of the transition dipole in the two dyes.

The angular range of local dye rotation was determined from a model of diffusion within a cone (Kinosita et al., 1977). The cone semi-angles (θ) for the fluorescein donor are ~36°, and the angles for tetramethylrhodamine acceptor are ~31° (Table III). Thus, both donor and acceptor dyes exhibit large rotational motions, with tetramethylrhodamine being slightly more restricted than fluorescein. The anisotropy decay data demonstrate that the local rotational dynamics of the dyes were identical in each labeled junction, regardless of which strand the dyes were attached to. These results confirm that the local dye environment was the same in each D–A junction.

On the basis of these estimates of rotational mobility of the donor and acceptor, the most probable values for the orientation factor, κ^2, are between 0.40 and 1.3 (Haas et al., 1978),

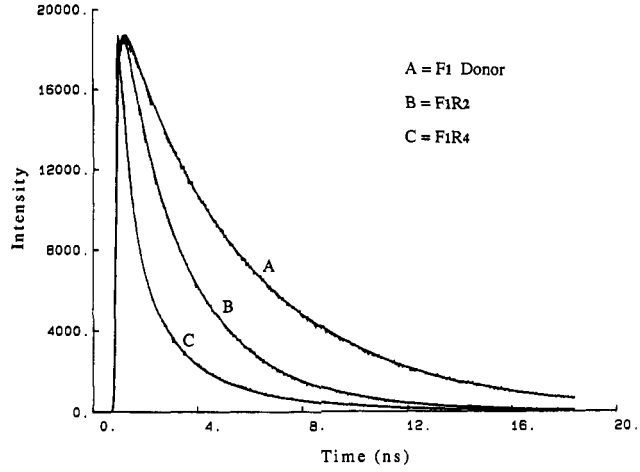

FIGURE 1: Fluorescence decay curves of the fluorescein donor in donor-only junction F1 (curve A), D–A junction F1R2 (curve B), and D–A junction F1R4 (curve C). The convention used for naming the dye-labeled junctions is given in the text (Materials and Methods). Donors were excited at 514.5 nm, and their fluorescence emission was observed at 530 nm. The decays are overlaid with best-fit curves in each case. In curve A, the best fit to eqs 4 and 5 with two donor lifetimes is shown. In curves B and C, the best fits to eq 12 are shown. The fits are indistinguishable from the experimental decays in each case.

corresponding to β_1 = 0.6 and β_2 = 2.0. Thus, the large-amplitude local rotational motions of the donor and acceptor dyes ensure that the orientation factor lies in a relatively narrow range of values close to the free rotation limit (β = 1). Orientational effects on energy transfer are therefore not expected to play a major role in the present system.

Donor–Acceptor Distance Distributions. Fluorescence decays of the fluorescein donor were measured in six different D–A junctions for calculation of the six interarm distance distributions. Figure 1 shows the quenching effect of the tetramethylrhodamine acceptor on the fluorescence decay of the fluorescein donor. The decay of the donor-only junction F1 is shown together with the decays of the D–A junctions F1R2 and F1R4. Clearly the donor fluorescence is quenched in the latter two junctions; however, energy transfer is greater in F1R4, reflecting a closer proximity of the donor and acceptor dyes.

The recovered D–A distance distributions are shown in Figure 2 for the F1R2 and F1R4 junctions. Distance distributions were calculated from eq 11 using the best fit values of a and b obtained from the donor decay analysis. Each distribution represents the probability that a particular D–A distance is present. It is evident that a much broader distribution of distances is obtained for the F1R4 junction than for the F1R2 junction. Parameters describing the distance distributions recovered for each D–A junction are reported in Table IV. The full width of the distribution at half-maximum probability (fwhm) is representative of the range of distances between the 5′ ends of the strands as reported by the donor and acceptor chromophores. The fwhm values of the F1R4 and F2R3 junctions are significantly larger than those obtained for any of the other four D–A junctions (Table IV). To verify the uniqueness of the Gaussian distribution analysis in these two junctions, we also tried fitting the donor decays with a single D–A distance or with two discrete D–A distances. The resulting fits with a single D–A distance were very poor, as indicated by the reduced χ-square values (χ_R^2 = 104 for F1R4 and χ_R^2 = 88 for F2R3). Furthermore, it was not possible to fit the decays with two discrete D–A distances, even when the two distances and their relative probabilities of occurrence were freely optimized (χ_R^2 = 6.2

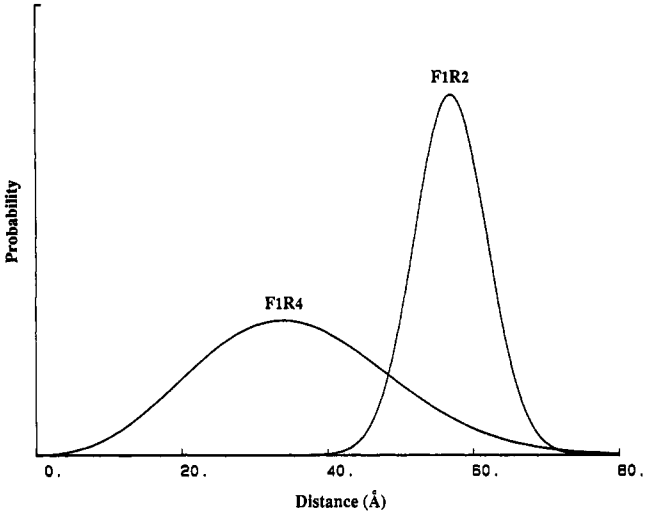

FIGURE 2: Gaussian D–A distance distributions in junctions F1R2 and F1R4 calculated from eq 11. The best fit values of a and b recovered from analysis of the corresponding donor decays were used in calculating the distributions. The distributions are normalized to unit area.

Table IV: D–A Distances in Dye-Labeled Four-Way Junctions

junction[a]	R_{ss} (Å)[b] (±0.5)	$\bar{R}$ (Å)[c] (±0.3)	fwhm (Å)[c] (±0.6)	β_1[d]	β_2[d]	χ_R^2
F1R2	55.6	55.0	13.1			1.10
		56.9	11.7	0.6	2.0	1.10
F1R3	56.0	57.2	18.4			1.13
		59.2	18.1	0.6	2.0	1.10
F1R4	42.1	34.5	31.4			1.25
		35.9	32.0	0.6	2.0	1.24
F2R3	43.9	36.2	28.6			1.13
		37.5	28.8	0.6	1.9	1.12
F2R4	56.1	55.9	15.5			1.03
		58.0	14.4	0.6	1.9	1.03
F3R4	54.8	55.8	14.6			1.01
		56.9	12.5	0.6	2.0	1.00
F3R2[e]	42.6	36.2	27.3			1.36
		38.5	28.1	0.6	2.0	1.35

[a] Each junction contains the indicated donor-labeled strand (F) and a 3-fold molar excess of unlabeled and acceptor-labeled (R) strands; refer to Chart I for strand sequences. [b] D–A distances determined from steady-state fluorescence measurements according to eq 3. [c] Parameters describing the D–A distance distribution obtained by fitting the donor's fluorescence decay according to eq 10 or 12. $\bar{R}$ is the mean D–A distance; fwhm is the full width of the distribution at half-maximum probability. The first entry for each D–A junction was obtained by fitting donor decays with eq 10, which assumes free rotation of the donor and acceptor. The second entry was obtained using eq 12, which averages the theoretical donor decay over a range of orientation factors consistent with the measured rotational mobilities of the donor and acceptor. The reduced χ-square values obtained for the best fits to eq 10 or 12 are indicated in the last column. D–A distance distributions were calculated with cutoff distances R_{min} = 3 Å and R_{max} = 80 Å. [d] β_1 and β_2 are the limits of orientational integration in eq 12. [e] Reverse measurement of F2R3.

for F1R4 and χ_R^2 = 4.8 for F2R3). In contrast, the Gaussian distributions gave excellent fits to the donor decays in these junctions, as indicated by the χ_R^2 values in Table IV (*e.g.*, χ_R^2 = 1.25 for F1R4).

The D–A distance distributions were calculated with cutoff distances R_{min} = 3 Å and R_{max} = 80 Å. These distances are estimates of the contact distance of the two fluorophores and the maximum possible D–A distance expected in the four-way junction (assumed to be the end-to-end distances along 16-bp stacking domains with the linkers in a fully extended conformation). We note that the recovered distributions do not depend on the precise values of the cutoff distances (*e.g.*, the same distributions were obtained with R_{min} = 1 or 5 Å and with R_{max} = 60 or 100 Å). Furthermore, inspection of the recovered distribution functions confirmed that these cutoff limits enclose the range of D–A distances in each labeled junction (Figure 2).

The donor decays were also analyzed with a Gaussian distribution of distances in one dimension. In this model, the $4\pi R^2$ term is absent from eq 11. The resulting distribution parameters, $\bar{R}$ and fwhm, were very similar to those reported in Table IV for a Gaussian distribution of distances in three dimensions. The only significant difference between the two models was that the one-dimensional distribution indicated a finite probability of D–A distances approaching R_{min}, whereas the probability of such short distances was negligible for the three-dimensional distribution.

Orientational effects on energy transfer were assessed by comparing D–A distance distributions recovered from either eq 10 or eq 12 (Table IV). Orientational effects are explicitly included in eq 12, based on the measured rotational mobility of the donor and the acceptor, whereas eq 10 is only strictly valid in the limit of free dye rotation. As mentioned earlier, the orientational dependence of energy transfer was not anticipated to have much effect on the D–A distance distributions, since both donor and acceptor motions were relatively unrestricted. This expectation is confirmed by the results in Table IV. For each junction, inclusion of the orientational dependence of energy transfer in the analysis of the donor decay had only a minor effect on the recovered distribution parameters: R increased by about 4%, and the fwhm values changed by only −1.4 to 0.8 Å. The orientational average in eq 12 assumes that all κ^2 values in the specified range are equally probable, which is probably an oversimplification. In any event, the effect of orientational averaging on the recovered distance distributions is small, and a more detailed treatment is not warranted. These results confirm that the recovered distribution parameters in Table IV do indeed reflect a range of distances between the dyes, rather than a range of orientations of the donor and acceptor transition dipoles.

A reverse measurement of the F2R3 distance distribution was made with D–A junction F3R2 to ensure that there was no preferential interaction of the dyes with the DNA which might bias the energy-transfer measurements. A 1.0-Å difference was observed in the $\bar{R}$ value, and a 0.7-Å difference was observed in the fwhm value. Thus, there does not appear to be any significant bias in the recovered D–A distance distributions.

The mean D–A distances reported in Table IV define the overall geometry of the four-way junction. As mentioned in the introduction, all the available evidence indicates that four-way junctions consist of two continuous domains formed by pairwise association of junction arms. Our observation of only two short D–A distances is consistent with a compressed X shape of the junction. The data in Table IV specify the arm-stacking arrangement and the relative orientation of the junction strands: arm I stacks with arm II, while arm III stacks with arm IV (Figure 3). On the basis of this arm-stacking arrangement, it follows that strands 1 and 3 are continuous within each stacking domain, while strands 2 and 4 are the crossover strands between stacking domains (Chart I). Furthermore, our data specify that the non-crossover strands are aligned antiparallel to one other. These stereochemical arrangements are the same as observed in the parental J1 junction (Churchill et al., 1988; Chen et al., 1993).

Steady-state FRET measurements also imply two short and four long D–A distances in a dye-labeled four-way junction (Murchie et al., 1989; Cooper & Hagerman, 1990). However, steady-state energy-transfer measurements will not provide

FIGURE 3: Simplified ribbon model of the antiparallel stacked-X structure of the four-way junction showing the arm-stacking arrangements identified in this study. The junction arms are labeled as in Chart I. Changes in the small angle between stacking domains, indicated by the curved arrows, would generate a range of distances along the long and short sides of the stacked X.

accurate interarm distances if a range of D–A distances are present in a given dye-labeled junction (Albaugh et al., 1989; Hochstrasser et al., 1992). We therefore compared the mean D–A distances recovered from the distribution analysis of the donor's fluorescence decay ($\bar{R}$) with the apparent D–A distances obtained from the donor's steady-state emission intensity (R_{ss}) in the same dye-labeled junctions (Table IV). It is thus apparent that steady-state FRET provides a reasonable approximation of the mean D–A distance when the distribution of distances is relatively narrow, as in the F1R2 and F3R4 junctions. However, steady-state energy transfer considerably overestimates the mean D–A distance when the distribution is broad, as in the F1R4 and F2R3 junctions. This may explain why the small angles in a four-way junction calculated from steady-state FRET measurements of the two short distances were larger than the corresponding angles measured by transient electric birefringence (Cooper & Hagerman, 1990), since the two shortest distances in the junction have the broadest distributions.

The most important aspect of our results is the large difference between the widths of the six interarm distance distributions in the four-way junction (Table IV). The end-to-end distances along the two stacking domains (junctions F1R2 and F3R4) exhibit the narrowest distributions (Figure 2). In contrast, the distances between adjacent ends of the stacking domains (junctions F1R4 and F2R3) exhibit very broad distributions (Figure 2). These results reveal a considerable degree of heterogeneity in the four-way junction structure, primarily involving the relative orientation of the two stacking domains.

The D–A distance distribution in the F1R4 junction was determined at several different temperatures and in a high-viscosity solvent to assess whether the junction was flexible. The mean D–A distances in the F1R4 junction did not vary significantly with temperature ($\bar{R}$ increased by only 1.0 Å between 5 and 30 °C), whereas the apparent fwhm of the distributions exhibited some temperature dependence, decreasing from 35.5 Å at 5 °C to 30.0 Å at 30 °C. The narrowing of the distribution at higher temperatures is consistent with increased diffusion of the donor and acceptor during energy transfer (Lakowicz et al., 1990). We note that orientational effects on energy transfer were accounted for in recovering D–A distance distributions at each temperature. Furthermore, the fraction of free donor species did not exceed 0.02 over the entire temperature range, indicating that the four-way junction remained intact at the higher temperatures. The mean D–A distance in 50% glycerol solution at 20 °C ($\bar{R}$ = 35.6 Å) was almost the same as that obtained for the F1R4 junction in aqueous buffer at the same temperature ($\bar{R}$ = 35.9 Å), whereas the distribution was broader in the glycerol solution: fwhm = 35.3 Å in glycerol solution compared with 32.0 Å in aqueous buffer. The broadening of the distribution is consistent with a decreased rate of donor–acceptor diffusion in the high-viscosity solvent. We note that changes in the intrinsic donor lifetimes, the rotational mobilities of the dyes, and the critical transfer distance were accounted for in recovering the D–A distance distribution in glycerol solution.

DISCUSSION

A variety of studies employing indirect structural techniques have shown that the four-way DNA junction folds into an X shape in the presence of cations (Cooper & Hagerman, 1987, 1989, 1990; Churchill et al., 1988; Duckett et al., 1988; Murchie et al., 1989). Since there is no direct structural data on the four-way junction, it is unknown whether this complex adopts a unique structure in solution. The time-resolved FRET technique used in the present study is also an indirect structural approach; yet it has the advantage of being able to resolve heterogeneous conformational distributions of the four-way junction. This is possible because the rate of resonance energy transfer between donors and acceptors attached to the junction arms depends strongly on the interarm distance, and a range of interarm distances gives rise to a characteristic nonexponential decay of the donor fluorescence. Thus, the presence of more than a single D–A distance is apparent in the form of the donor decay, whereas steady-state measurements of FRET based on the integrated emission intensity of the donor or acceptor do not provide such a direct indication of distance heterogeneity.

Using this approach, we have shown that none of the six D–A distances in the dye-labeled junctions have unique values. Instead, our results show that a range of D–A distances is present between each pair of labeled junction arms. Several effects could contribute to the observed distributions of D–A distances in the dye-labeled junctions. First, flexibility in the hexyl chains linking the dyes to the oligonucleotide strands could cause some variation in all the D–A distances. Second, fraying at the ends of the labeled junction arms could also produce some variation in the dye positions. Third, flexing of the arms could result in motion of the dyes at the ends of the arms. Fourth, interconversion between the four possible isomers of the stacked-X structure could generate a range of D–A distances between certain pairs of labeled junction arms. Finally, variation in the angle between the two stacking domains could generate a range of distances between all pairs of junction arms, except between the stacking partners.

Flexibility of the linkers and fraying of the junction arms will contribute to the D–A distance distribution in all six D–A junctions. Therefore, these effects cannot account for the large differences in the fwhm values of the six D–A distance distributions (Table IV), since the linkers and the terminal base pairs were the same in all labeled junctions. Direct measurement of local rotational motions of the dyes confirmed that dye flexibility was indeed the same at each arm terminus (Table III). On the basis of measurements of end-to-end energy transfer along a short DNA duplex containing the

same dye–linker/terminal base pair combinations as used here, linker flexibility and arm fraying are together estimated to contribute about 12 Å to the fwhm value of each D–A distance distribution in the junction (Hochstrasser et al., 1992). Interestingly, the D–A distance distributions measured along the two stacking domains have fwhm values close to this estimate (11.7 and 12.5 Å for F1R2 and F3R4 junctions, respectively), implying that the distributions reflect these intrinsic effects only. Thus, the junction arms themselves appear to be relatively rigid. However, two of the four remaining interarm distributions are considerably broader, reflecting the contribution of one or more of the other effects noted above.

The four isomers of a stacked-X structure result from two possible stacking arrangements (crossover isomers) and two possible orientations of the non-crossover strands (parallel or antiparallel). Although the set of mean D–A distances in Table IV are consistent with a single predominant isomer, the fwhm values may reflect the presence of minor populations of alternative isomers. For example, the distance between the ends of arms I and II would be different for each crossover isomer, while the distance between arms I and III would be similar for both isomers. Therefore, if the D–A distance distributions reflect transitions between crossover isomers, the F1R2 junction should exhibit a broader distribution than the F1R3 junction. Our data (Table IV) thus indicate that the junction forms only a single crossover isomer. Transitions between parallel and antiparallel isomers can account for the narrow distance distributions along stacking domains, since these transitions reverse the relative orientation of the two stacking domains while keeping the lengths of the domains fixed. However, it is not obvious why these transitions would produce a broader distribution of distances in the F1R4 junction than in the F1R3 junction (Table IV). Furthermore, the mean D–A distances between stacking domains would vary with temperature, reflecting changes in the relative isomer populations. For example, an increase in temperature should favor the minor parallel isomer. Since the parallel isomer of the F1R4 junction would have a larger D–A distance than the antiparallel isomer, the mean D–A distance ($\bar{R}$) should increase at higher temperatures if both isomers are significantly populated. However, no significant change in $\bar{R}$ was detected in the F1R4 junction between 5 and 30 °C, indicating that the antiparallel isomer was the predominant species present under these conditions.

An ensemble of stacked-X structures, characterized by a range of angles between two rigid stacking domains, can account for the range of distances present between each pair of arms in the four-way junction. The end-to-end distances along the stacking domains would be well defined in such an ensemble, but a range of distances would be present between the stacking domains (Figure 3). Accordingly, the narrowest distance distributions are observed in the F1R2 and F3R4 junctions (Table IV). In addition, angular variations in a stacked-X structure would produce a greater variation in the distance across the short side of the X compared with the longer side. For example, a simple trigonometric argument based on a planar X geometry reveals that, for a given change in the small angle in the X, the distance along the short side changes more than does the distance along the long side. In fact, the broadest distance distributions do correspond to the two shortest distances between stacking domains (junctions F1R4 and F2R3; Table IV).

An ensemble of stacked-X structures in solution is consistent with molecular mechanics calculations, which show that sterically acceptable four-way junctions can be formed with a wide range of angles between the stacking domains (Srinivasan & Olson, 1993). Our results suggest that the energy differences between these structures are relatively small, such that a distribution of structures is thermally populated in solution. Furthermore, the formation of closed cyclic trimers and tetramers by enzymatic ligation of four-way junctions also implies that the branch angles can adopt different values (Petrillo et al., 1988).

The small angles between stacking domains in the four-way junction have been estimated using various physical methods, and values around 60° have been reported for different junctions (Lilley & Clegg, 1993). We note that the mean D–A distances in Table IV are also consistent with these estimates. However, since our results reveal that the small angles are actually described by distributions, it appears that these estimates should be interpreted as the average angles present in a family of junction conformations, rather than as reflecting a unique junction structure.

The ability of the stacking domains to adopt different relative orientations suggests that the junction may be flexible in solution. As a first step toward characterizing the flexibility of the four-way junction, we have examined the effect of temperature and solvent viscosity on the recovered D–A distance distributions in the F1R4 junction. Since the dyes are located on adjacent ends of the stacking domains in this junction (Figure 3), their separation is sensitive to changes in the relative orientation of the domains, as noted above. We found that the fwhm value of the recovered distribution decreased as temperature increased, while the mean D–A distance remained nearly constant. This behavior is consistent with an increased rate of diffusive motions of the donor and acceptor. These motions partially average the distribution of D–A distances prior to energy transfer, such that the recovered distribution appears to have narrowed (Lakowicz et al., 1990; Amir & Haas, 1987). In addition, the recovered D–A distribution in a 50% glycerol solution was broader than in aqueous solution, reflecting a decreased rate of D–A diffusion in the higher viscosity solvent. Thus, the temperature and solvent effects both indicate that the junction is flexible. However, the effects of this flexibility on the recovered distribution widths are relatively small. Thus, the static distribution analysis presented here is suitable for examining the conformational distributions of the four-way junction. Flexibility of the junction can be evaluated in more detail by additional temperature and viscosity studies in each labeled junction and by including diffusion terms in the analysis of the donor decay (Lakowicz et al., 1991). These studies are in progress and will be reported elesewhere.

CONCLUSIONS

Time-resolved FRET measurements have revealed that the four-way DNA junction does not adopt a unique structure in solution. Several explanations for the distribution of distances present between each pair of junction arms have been considered. An ensemble of stacked-X structures, characterized by differences in the angle between the two stacking domains, accounts for all the experimental observations. Thus, it appears that considerable conformational variability can exist within a single crossover and rotational isomer of the four-way junction. In addition, our results give an indication that the four-way junction is flexible in solution. The results of this study illustrate the advantage of using fluorescence decay measurements combined with distance distribution analysis when FRET is applied to conformationally heterogeneous nucleic acid structures.

REFERENCES

Albaugh, S., & Steiner, R. F. (1989) *J. Phys. Chem. 93*, 8013–8016.

Albaugh, S., Lan, J., & Steiner, R. F. (1989) *Biophys. Chem. 33*, 71–76.

Amir, D., & Haas, E. (1987) *Biochemistry 26*, 2162–2175.

Beardsley, K., & Cantor, C. R. (1970) *Proc. Natl. Acad. Sci. U.S.A. 65*, 39–46.

Bevington, P. R. (1969) *Data Reduction and Error Analysis for the Physical Sciences*, McGraw-Hill, New York.

Cardullo, R. A., Agrawal, S., Flores, C., Zamecnik, P. C., & Wolf, D. E. (1988) *Proc. Natl. Acad. Sci. U.S.A. 85*, 8790–8794.

Chen, S.-M., Heffron, F., Leupin, W., & Chazin, W. J. (1991) *Biochemistry 30*, 766–771.

Chen, S.-M., Heffron, F., & Chazin, W. J. (1993) *Biochemistry 32*, 319–326.

Churchill, M. E. A., Tullius, T. D., Kallenbach, N. R., & Seeman, N. C. (1988) *Proc. Natl. Acad. Sci. U.S.A. 85*, 4653–4656.

Cooper, J. P., & Hagerman, P. J. (1987) *J. Mol. Biol. 198*, 711–719.

Cooper J. P., & Hagerman, P. J. (1989) *Proc. Natl. Acad. Sci. U.S.A. 86*, 7336–7340.

Cooper, J. P., & Hagerman, P. J. (1990) *Biochemistry 29*, 9261–9268.

Cooper, J. P., & Hagerman, P. J. (1991) *Curr. Opin. Struct. Biol. 1*, 464–468.

Cross, A. J., & Fleming, G. R. (1984) *Biophys. J. 46*, 45–56.

Demas, J. N., & Crosby, G. A. (1971) *J. Phys. Chem. 75*, 991–1024.

Duckett, D. R., Murchie, A. I. H., Diekmann, S., von Kitzing, E., Kemper, B., & Lilley, D. M. J. (1988) *Cell 55*, 79–89.

Eis, P. S., & Lakowicz, J. R. (1993) *Biochemistry 32*, 7981–7993.

Förster, T. (1949) *Z. Naturforsch. A4*, 321–327.

Guo, Q., Lu, M., Seeman, N. C., & Kallenbach, N. R. (1990) *Biochemistry 29*, 570–578.

Haas, E., Wilchek, M., Katchalski-Katzir, E., & Steinberg, I. Z. (1975) *Proc. Natl. Acad. Sci. U.S.A. 72*, 1807–1811.

Haas, E., Katchalski-Katzir, E., & Steinberg, I. Z. (1978) *Biochemistry 17*, 5064–5070.

Hochstrasser, R. A., Chen, S.-M., & Millar, D. P. (1992) *Biophys. Chem. 45*, 133–141.

Holliday, R. (1964) *Genet. Res. 5*, 282–304.

Kallenbach, N. R., Ma, R.-I., & Seeman, N. C. (1983) *Nature 305*, 829–830.

Kinosita, K., Kawato, S., & Ikegami, A. (1977) *Biophys. J. 20*, 289–305.

Lakowicz, J. R., Gryczynski, I., Cheung, H. C., Wang, C.-K., Johnson, M. L., & Joshi, N. (1988) *Biochemistry 27*, 9149–9160.

Lakowicz, J. R., Wiczk, W., Gryczynski, I., Szmacinski, H., & Johnson, M. L. (1990) *Biophys. Chem. 38*, 99–109.

Lakowicz, J. R., Kusba, J., Wiczk, W., Gryczynski, I., Szmacinski, H., & Johnson, M. L. (1991) *Biophys. Chem. 39*, 79–84.

Lilley, D. M. J., & Clegg, R. M. (1993) *Annu. Rev. Biophys. Biomol. Struct. 22*, 299–328.

Millar, D. P., Hochstrasser, R. A., Guest, C. R., & Chen, S.-M. (1992) *Proc. SPIE -Int. Soc. Opt. Eng. 1640*, 592–598.

Murchie, A. I. H., Clegg, R. M., von Kitzing, E., Duckett, D. R., Diekmann, S., & Lilley, D. M. J. (1989) *Nature 341*, 763–766.

Petrillo, M. L., Newton, C. J., Cunninghamn, R. P., Kallenbach, N. R., & Seeman, N. C. (1988) *Biopolymers 27*, 1337–1352.

Seeman, N. C. (1982) *J. Theor. Biol. 99*, 237–247.

Seeman, N. C., & Kallenbach, N. R. (1983) *Biophys. J. 44*, 201–209.

Srinivasan, A. R., & Olson, W. K. (1993) *Biophys. J. 64*, A11.

von Kitzing, E., Lilley, D. M. J., & Diekmann, S. (1990) *Nucleic Acids Res. 18*, 2671–2683.

Wemmer, D. E., Wand, A. J., Seeman, N. C., & Kallenbach, N. R. (1985) *Biochemistry 24*, 5745–5749.

Wu, P. G., Rice, K. G., Lee, Y. C., & Brand, L. (1991) *Proc. Natl. Acad. Sci. U.S.A. 88*, 9355–9399.

Yang, C.-H., & Söll, D. (1974) *Proc. Natl. Acad. Sci. U.S.A. 71*, 2838–2842.